J Therm Anal Calorim (2015) 119:319–327
DOI 10.1007/s10973-014-4137-0

# Thermal characterization of II–VI binary crystals by photopyroelectric calorimetry and infrared lock-in thermography

**K. Strzałkowski · M. Streza · D. Dadarlat · A. Marasek**

Received: 3 March 2014 / Accepted: 26 August 2014 / Published online: 24 September 2014


**Abstract** In this paper, a complete thermal characterization (measurement of all static and dynamic thermal parameters) of some selected II–VI binary crystals was carried out. The semiconductors under investigation were grown from the melt by high-pressure/high-temperature-modified Bridgman method. The contact photopyroelectric (PPE) method in back configuration and non-contact infrared lock-in thermography technique were used in order to get the thermal diffusivity of the investigated crystals. The thermal effusivity of the samples was obtained using the PPE technique in the front configuration, together with the thermal wave resonator cavity method. Knowing the values of the thermal effusivity and thermal diffusivity, the remaining two thermal parameters, i.e., thermal conductivity and specific heat were calculated.

**Keywords** II–VI binary crystals · Lock-in thermography · PPE method · Thermal characterization

## Introduction

II–VI semiconductors are considered as very promising materials largely used as visible radiation sources in green laser diodes, in spintronics, photodetection, and other applications in modern optoelectronics [1]. The binary crystals investigated in this work (ZnSe, ZnTe, CdSe and CdTe) can be treated as starting materials for mixed solid solutions. From the application point of view, the main feature of the ternary and quaternary II–VI compounds consists in the possibility of smooth changes in bandgap and lattice constant values [2]. Thermal characterization of these materials is very important due to the dissipation of the heat in miniaturized semiconducting devices. Thermal parameters are unique for each material, being strongly dependent on the composition, structural characteristics and fabrication process. The aim of this paper is to perform a complete thermal characterization of the investigated materials by measuring/calculating all static (specific heat) and dynamic (thermal diffusivity, effusivity and conductivity) thermal parameters. To get this, several experimental techniques were used.

PPE technique has been extensively applied to the study of thermal properties of condensed matter samples [3–6]. The major advantages of this technique are its simplicity, high sensitivity, non-destructive character, and adaptation on experimental restrictions for theoretical requirements. In classical back configuration (BPPE) method, for the investigation of solid samples, a coupling fluid must be introduced between the sample and sensor in order to ensure a good thermal contact. This always leads to an error in thermal diffusivity measurement. This fact is in agreement with the results obtained by Salazar et al. [7–9]. They have been shown that the results obtained with BPPE technique are always underestimated due to the presence of the coupling fluid between the sample and the sensor. The influence of the coupling fluid in pyroelectric measurements of solids becomes significant especially for high conductive samples and at high modulation frequency of incident radiation. One of the solutions to tackle this

K. Strzałkowski · A. Marasek
Faculty of Physics, Astronomy and Informatics, Institute of Physics, Nicolaus Copernicus University, Grudziadzka 5, 87-100 Torun, Poland

M. Streza (✉) · D. Dadarlat
National R&D Institute for Isotopic and Molecular Technologies, Donath Str. 65-103, POB-700, 400293 Cluj-Napoca, Romania
e-mail: streza.mihaela@gmail.com

problem could be a non-contact technique as infrared lock-in thermography.

In fact the PPE technique, in a combined back and front configuration is able to find both thermal diffusivity and effusivity of the investigated samples. The necessity of using a second, non-contact technique is generated by the presence of the coupling fluid in the PPE technique. It is well known that the coupling fluid influences more or less the quantitative results, depending on parameters such as chopping frequency, thickness of various layers of the detection cell, etc. In the front configuration, the influence of the coupling fluid was eliminated using the thermal wave resonator cavity (TWRC) method [10]. However, this is not possible in the back configuration and this is why a second non-contact technique (lock-in thermography) is proposed in order to increase the accuracy of thermal diffusivity measurements, by eliminating the influence of the coupling fluid.

## Materials and methods

The crystals under investigation were grown from the melt by the high-pressure (150 atm of Argon) modified vertical Bridgman method using high purity (99.995 %) powders of ZnSe, ZnTe, CdSe, and CdTe, in a graphite crucible. The crystal rods (1 cm in diameter) were cut into about 1.5-mm-thick plates. The samples were first ground using the grinding powder ($Al_2O_3$, 10 μm in diameter) and next polished with the diamond paste (1 μm). All the samples had a cylindrical shape. The geometrical parameters of the samples were measured with a micrometer with an accuracy of 10 μm. The samples were weighed with a Discovery OHAUS laboratory analytical balance designed to measure small mass in the sub-milligram range (i.e., the sensitivity of the balance is 0.1 mg).

For PPE investigations, a typical experimental setup in the back configuration was used [11]. It consisted of a 50 mw power DPSS laser ($\lambda = 532$ nm), a 0.54-mm-thick $LiTaO_3$ detector, provided with CrAu electrodes and a SR830 lock-in amplifier. The reference signal provided from the internal oscillator of the lock-in was used for the modulation of the incident radiation. In BPPE configuration, the sample (placed onto the sensor) is directly excited with a modulated radiation. A thin layer of ethylene glycol served as a coupling fluid between the sample and the sensor. To protect the detector from direct illumination, a black diaphragm was used. All samples (transparent or opaque) have been blackened with a thin carbon layer, in order (i) to assure the optical opacity of the transparent samples and (ii) to avoid the influence of an optical excited state of the semiconductor on its thermal properties (phonon scattering processes on free excited carriers). Because the deposited carbon layer is very thin (<1 μm) and has a high thermal conductivity, one can neglect its influence on the signal. The modulation frequency of the excitation source was changed in the range of 0.2–15 Hz.

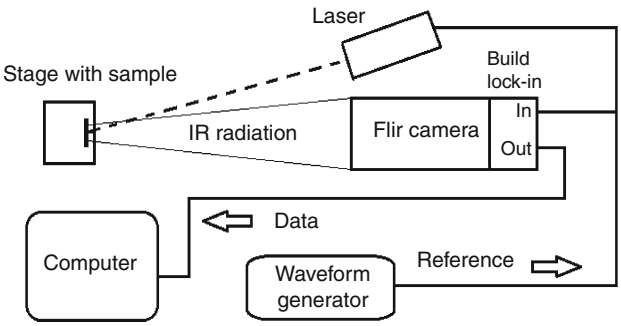


**Fig. 1** Experimental setup for the lock-in thermography technique

In the front configuration (FPPE), coupled with the thickness scanning procedure (TWRC), the radiation source was a red He–Ne laser (Melles Griot, 35 mW, $\lambda = 632$ nm) modulated with an acousto-optical modulator. A LiTaO3 crystal (with a thickness of 215 μm), coated with a CrAu film, was used as pyroelectric sensor, and a SR830 lock-in amplifier collected the signal from the electrodes [12]. In this method, the laser directly illuminates the sensor. The specimens were placed into the detection cell in the back position. Ethylene glycol with known thermal properties was inserted as coupling fluid between the sample and the sensor. The initial thickness of ethylene glycol was about 0.5 mm. The liquid was compressed during the thickness scan procedure. The scanning procedure was performed by a 9062 M-XYZ-PPP Gothic-Arch-Bearing Picomotor with a single step of 6 μm. The parallelism between the backing and the sensor was assured by means of 3-axis and 6-axis micrometric stages.

The experimental IR setup included a heat source, a waveform generator, an infrared camera, and a computer for data acquisition (Fig. 1). The intensity-modulated optical stimulation ($f_0 = 2$ Hz) was delivered by a Nd:YAG laser (Laser Quantum OPUS, with $\lambda = 532$ nm and internally modulated power which was set at $P = 500$ mW). The IR camera (FLIR 7,200 series, with a 256 × 320 pixel array of InSb detectors sensitive in the 1.5–5.1 μm wavelength range, working at a sampling frequency of 100 Hz) recorded the changes in the surface temperature of the specimens. The noise equivalent temperature difference (NETD) of this camera is lower than 20 mK. The signals delivered by the infrared camera and the reference frequency $f_0$ were sent to the lock-in detection module incorporated into the camera, which outputs the continuous component image ($f = 0$) as well as the amplitude and phase images of the $f$-component to a PC.

The optical axis of the camera was perpendicular to the investigated surface.

A glassy-like carbon (GC) type G (1 mm thickness) with known thermal parameters was selected as a reference sample [13]. All the measurements have been performed at room temperature. The frequency/thickness variation and control and the data acquisitions were computer-controlled.

## Theory

The BPPE configuration cell consists of four-layers disposed as follows: air/opaque sample/pyroelectric sensor/air. Assuming a perfect thermal contact between the sample and the sensor and the one-dimensional model of the heat propagation through the sandwich-type system, the complex PPE signal is given by [14, 15]:

$$V = \frac{2V_0 e^{-\sigma_s L_s}}{b_{sp}+1}\frac{1-e^{-2\sigma_p L_p}}{1+R_{sp}e^{-2\sigma_p L_p}-(R_{sp}+e^{-2\sigma_p L_p})e^{-2\sigma_s L_s}} \quad (1)$$

In Eq. 1, $V_0$ is an instrumental factor, *ij* represents *s* and *p* layers of the detection cell, respectively.

$$R_{ij} = (b_{ij}-1)/(b_{ij}+1) \quad (2)$$

is the reflection coefficient of the thermal wave at *ij* interface, $b_{ij} = e_i/e_j$ and *e* is thermal effusivity.

$$\sigma_i = (1+i)a_i \quad (3)$$

is the complex diffusion coefficient.

$a_i$ is the reciprocal of the thermal diffusion length $\mu_i$

$$a_i = 1/\mu_i \quad (4)$$

$$\mu_i = (2\alpha_i/\omega)^{1/2} \quad (5)$$

$\omega$ is the angular modulation frequency and $L_i$ is the thickness of the layer *i*. In order to eliminate the instrumental factor $V_0$, the useful signal is normalized with respect to the signal obtained with the empty sensor [12]. After the normalization procedure and assuming the thermally thick regime for both the detector and the sample ($\mu_i < L_i$), one can calculate the thermal diffusivity using the amplitude (Eq. 6) and/or the phase (Eq. 7) of the complex signal [12]:

$$\ln|V_n| = \ln\frac{2}{b_{sp}+1} - a_s L_s \quad (6)$$

$$\Theta = \Theta_0 - L_s\left(\frac{\omega}{2\alpha_s}\right)^{1/2} \quad (7)$$

The amplitude is affected by external factors, such as laser-intensity fluctuations and the roughness of the surface, whereas the phase provides more accurate results, being independent on these external factors. For this reason, the thermal diffusivity was calculated according to Eq. 7, the excitation frequency being used as scanning parameter.

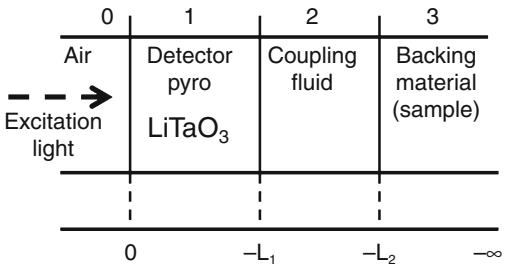


**Fig. 2** The cell's model in the front configuration for the TWRC method

The FPPE-TWRC configuration (see Fig. 2) consists of four layers disposed in the following order: air/pyroelectric sensor/coupling fluid/sample. In a one-dimensional heat propagation model, the normalized complex PPE signal is given by [10]:

$$V_n = \frac{1-R_{21}e^{-2\sigma_1 L_1}}{1-\rho_{21}e^{-2\sigma_1 L_1}}\frac{(e^{-\sigma_1 L_1}-1)-\rho_{21}(e^{-\sigma_1 L_1}-e^{-2\sigma_1 L_1})}{(e^{-\sigma_1 L_1}-1)-R_{21}(e^{-\sigma_1 L_1}-e^{-2\sigma_1 L_1})}, \quad (8)$$

where

$$R_{21} = \frac{1-b_{21}}{1+b_{21}}, \quad (9)$$

$$\rho_{21} = \frac{(1-b_{21})+\rho_{32}(1+b_{21})e^{-2\sigma_2 L_2}}{(1+b_{21})+\rho_{32}(1-b_{21})e^{-2\sigma_2 L_2}}, \quad (10)$$

$$\rho_{32} = \frac{1-b_{32}}{1+b_{32}} \quad (11)$$

The main advantage of this configuration, compared to the classical frequency scanning methods, is connected with the possibility of controlling the type and the thickness variation of the coupling fluid [12]. Moreover, no additional normalization is required (according to Eq. 8); normalization signal is contained in the same scanning run (thermally very thick regime for the scanned liquid) and consequently, no additional measurement is necessary. Basically, in this configuration, one can get the thermal parameters of each layer of the detection cell (if the thermal parameters of the other layers are known). In this paper, we focused only on the thermal effusivity of the sample inserted as backing in the detection cell. The thermal diffusivity and effusivity values of the other layers [16] taken into the theoretical calculations were (i) for $LiTaO_3$

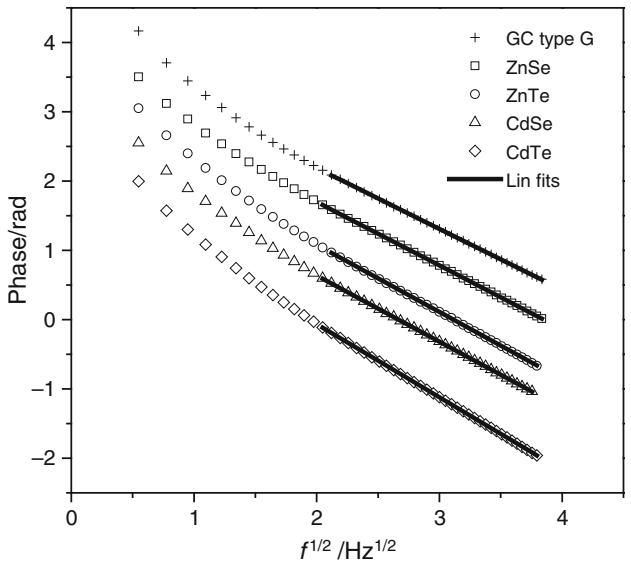


**Fig. 3** The BPPE phases in radians of all investigated samples as a function of the square root of the modulation frequency, *points* are experimental data and *lines* are linear fits

detector: $1.36 \times 10^{-6}$ m$^2$ s$^{-1}$ and 3,660 W s$^{1/2}$ m$^{-2}$ K$^{-1}$, (ii) for ethylene glycol: $9.36 \times 10^{-8}$ m$^2$ s$^{-1}$ and 814 W s$^{1/2}$ m$^{-2}$ K$^{-1}$.

The theoretical model for thermal diffusivity measurement of solid samples by lock-in thermography is presented below. The heat wave equation generated by a time-periodic punctual heat source in an isotropic and homogeneous medium with thermal diffusivity $\alpha$, can be written as [17]:

$$T(x,t) = T_0 e^{j(2\pi ft - \vec{k}\vec{x})}, \tag{12}$$

where $\vec{x}$ is the thermal wave propagation direction, $T_0$ is the surface temperature, $f$ is the excitation frequency, $t$ is the time, and $\vec{k}$ is the wave vector. The 1-D thermal diffusion equation is given by:

$$\alpha \frac{\partial^2 T(x,t)}{\partial x^2} = \frac{\partial T(x,t)}{\partial t}, \tag{13}$$

where

$$k = \pm(1-j)\sqrt{\frac{\pi f}{\alpha}} \tag{14}$$

For physical reasons, the thermal wave must converge at infinity, which requires

$$k = (1-j)\sqrt{\frac{\pi f}{\alpha}} \tag{15}$$

The thermal wave can be written as follows:

$$T(x,t) = T_0 e^{-\sqrt{\frac{\pi f}{\alpha}}x} e^{j\left(2\pi ft - \sqrt{\frac{\pi f}{\alpha}}x\right)} \tag{16}$$

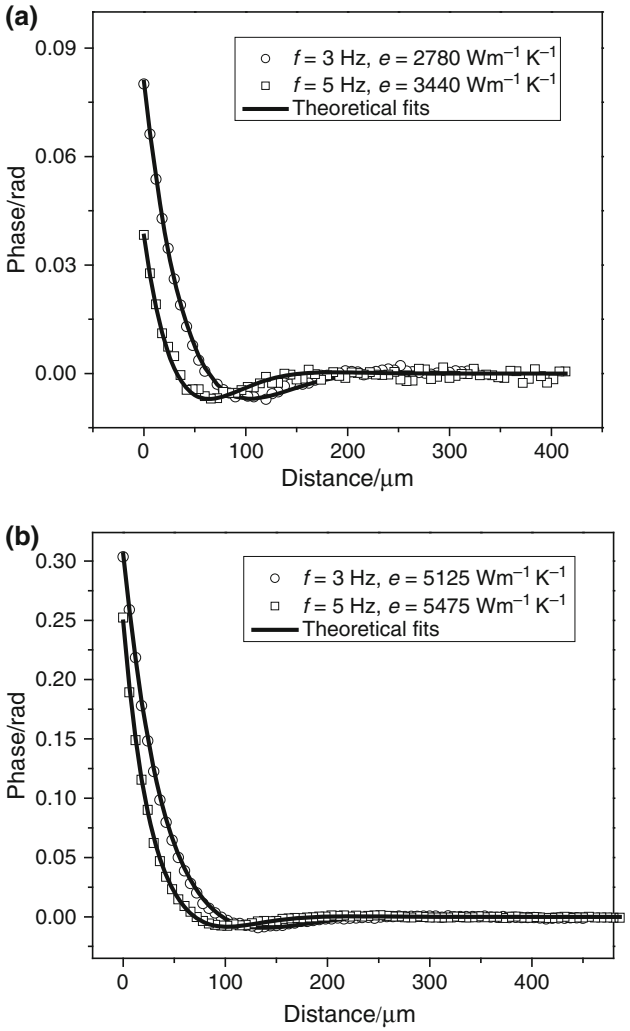


**Fig. 4** The phase characteristics of the glassy-like carbon (**a**) and ZnSe (**b**) samples measured at 3 (*circles*) and 5 Hz (*squares*), respectively, with the *thickness* scan procedure in the front configuration, *points* represent experimental results and *lines* are theoretical fittings

The propagation of a plane thermal wave through a medium of the thickness $x$ and the thermal diffusivity $\alpha$ causes a phase shift $\Delta\varphi$ (a delay in the propagation of thermal wave as compared to a reference signal) having the following expression:

$$\Delta\phi = -\sqrt{\frac{\pi f}{\alpha}}x = ax, \tag{17}$$

where $a$ is the slope of the phase-distance graph. The thermal diffusion length is expressed by:

$$\mu = \frac{1}{a} = \sqrt{\frac{\alpha}{\pi f}} \tag{18}$$

At a big distance from the punctual heat source, the thermal wave can be approximated by a plane wave and

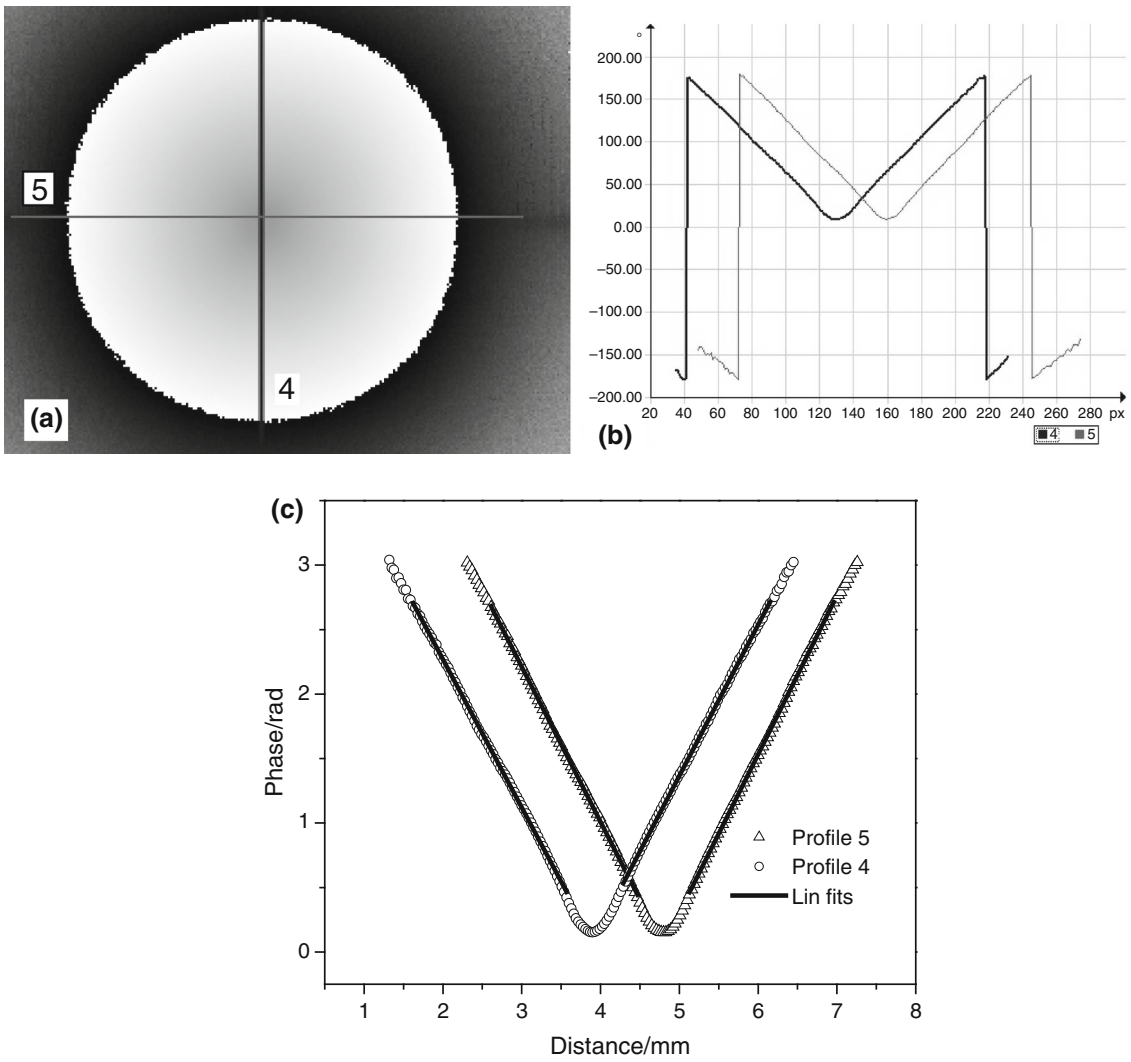


**Fig. 5** Thermal image of the phase of the glassy-like carbon (**a**) sample measured at 2 Hz and corresponding phase profiles (**b**, **c**) taken from the thermal images, circles correspond to the measured data and lines are linear fits; **b** *Ox* axis: coordinate (*pixel*); *Oy* axis: phase (*deg*)

thus, the thermal diffusivity can thus be calculated according to Eq. 18.

## Results and Discussion

Figure 3 presents the behavior of the phase as a function of the square root of the modulation frequency (in BPPE configuration), for all investigated samples. For low frequencies the curves exhibit a non-linear dependence due to the thermally thin regime of the sample or/and the sensor. Starting from $f = 4$ Hz, the sensor and all samples are thermally thick. Consequently, linear fits have been performed in the frequency range of 4–15 Hz, using the least square method. Thermal diffusivities were calculated according to Eq. 7.

Figure 4 reveals the phase behavior of glassy-like carbon and ZnSe samples, with theoretical fits, using the thickness scanning procedure of the coupling fluid in FPPE configuration. At 3 and 5 Hz, the sensor and the coupling fluid are thermally thin and the sample is thermally thick, the theoretical conditions being fulfilled. The constant behavior of the phase in Fig. 4 is associated to the thermally thick regime of the coupling fluid, and it is used for the normalization procedure. In order to obtain the thermal effusivity, a numerical analysis of Eq. 8 has been performed (the method of least squares) with two fit parameters: the thermal effusivity of the backing material (sample), and the absolute thickness of the coupling fluid (distance between the sample and the sensor). The best theoretical fits and obtained values of thermal effusivity are also displayed in Fig. 4.

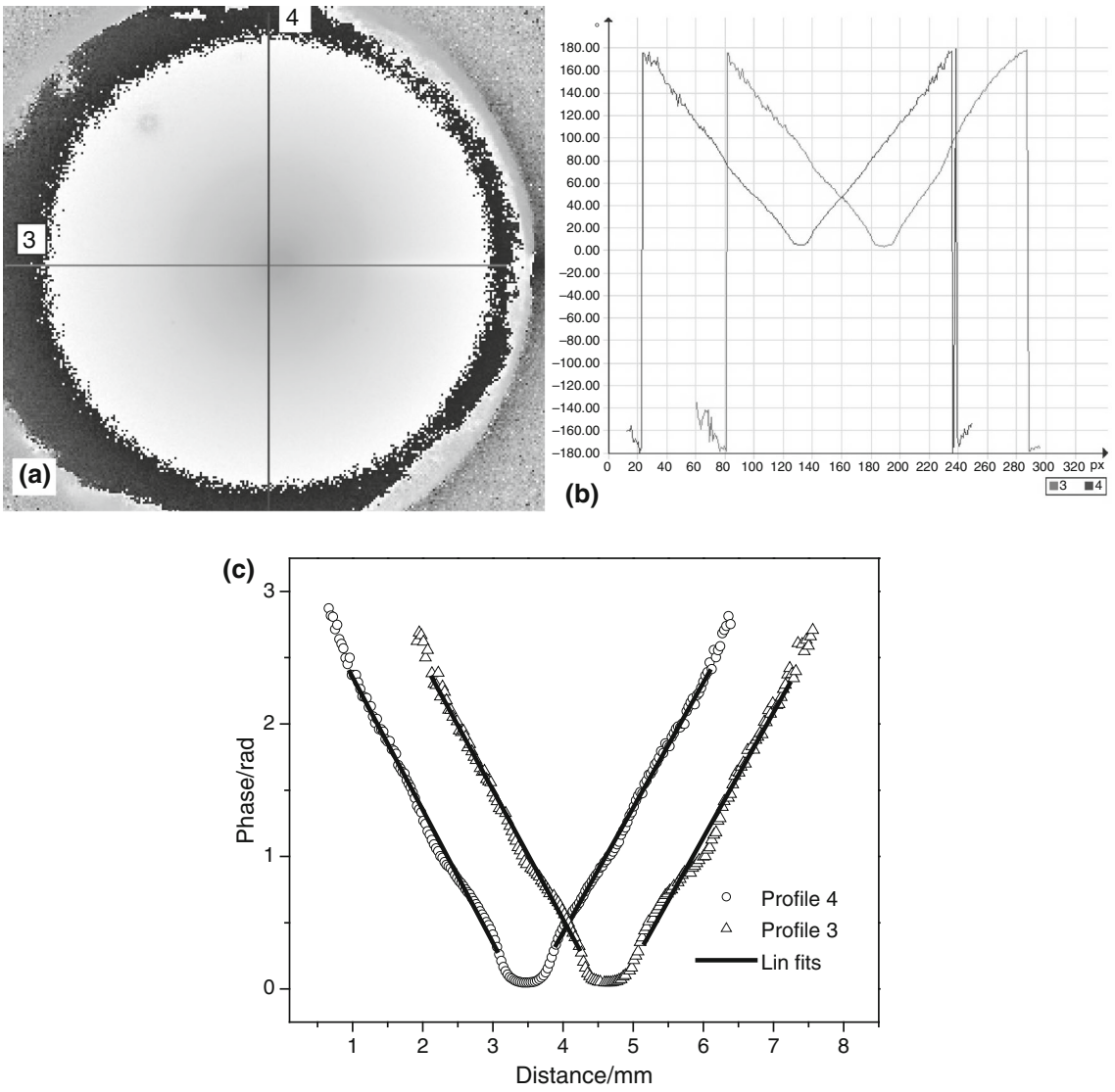


**Fig. 6** Thermal image of the phase of the ZnSe (**a**) sample measured at 2 Hz and corresponding phase profiles (**b**, **c**) taken from the thermal images, **circles** correspond to the measured data and lines are linear fits; **b** *Ox* axis: coordinate (*pixel*); *Oy* axis: phase (*deg*)

Phase images for glassy-like carbon and ZnSe with the corresponding profiles are shown in Fig. 5 (a–c) and Fig. 6 (a–c), respectively, The impact zone of the laser is represented by the constant phase zones. The thermal wave is propagating continuously, normal to the observed object surface, symmetrically with respect to the excitation point-source. The diameter of the laser is about 150 μm (1px = 30 μm). The thermal wave spreads on the surface over a distance of about 3 mm around the excitation source. At this distance from the excitation source, the spherical thermal wave can be approximated by a plane wave. The phase shift +180° to −180° is due to the displaying mode after lock-in detection. If such a phase shift occurs, a +360° phase-correction must be applied. Under coordinate $x = 60$px and, respectively, over coordinate $x = 260$px (see Fig. 5b, profile 5, for instance), the signal becomes noisy (meaning that the thermal wave is attenuated).The useful signal is between $x = 60$px and $x = 260$px. The thermal diffusivity was calculated from phase profiles, according to Eq. 18.

In our experiment, the thermal diffusion length (1 mm) is comparable to the thickness of the disk (about 1.5 mm). Consequently, it seems that the thermally thick regime for the sample is not fulfilled. However, as demonstrated before Chirtoc [18], the adjacent layers of the investigated sample can generate an effective thermal thickness of the sample much larger than the geometrical one. In our experiment, the sample is a self-supporting relatively thin semiconductor in air. For large thermal effusivity mismatch (in our case the thermal effusivity is around 3,000 W $s^{1/2}$ $m^{-2}$ $K^{-1}$ for semiconductor and 5 W $s^{1/2}$ $m^{-2}$ $K^{-1}$ for air), the

**Table 1** Thermal parameters of the investigated binary crystals and the GC sample type G

| | ZnSe (c) | ZnTe (c) | CdSe (h) | CdTe (c) | GC G |
|---|---|---|---|---|---|
| Thermal conductivity[a]/W $m^{-1}$ $K^{-1}$ | 19 | 18 | 9 | 7.1 | 6.3 |
| Thermal conductivity/W $m^{-1}$ $K^{-1}$ | 13.4 | 9.31 | 4.55 | 4.51 | 6.34 |
| Thermal diff. averaged/$m^2$ $s^{-1}\times10^{-6}$ | 6.41 | 7.5 | 3.57 | 3.1 | 4.15 |
| Thermal diff. camera/$m^2$ $s^{-1}\times10^{-6}$ | 6.73 | 7.87 | 3.6 | 3.14 | 4.4 |
| Thermal diff. from PPE/$m^2$ $s^{-1}\times10^{-6}$ | 6.1 | 7.1 | 3.55 | 3.05 | 3.91 |
| Thermal effusivity/W $s^{1/2}$ $m^{-2}$ $K^{-1}$ | 5,300 | 3,400 | 2,420 | 2,560 | 3,110 |
| Specific heat/J $kg^{-1}$ $K^{-1}$ | 420.9 | 235.4 | 239 | 264.3 | 1,075.1 |
| Density/kg $m^{-3}$ | 5,016.5 | 5,275 | 5,401 | 5,501 | 1,420[a] |

[a] Values taken from the literature for cubic (c) and hexagonal (h) crystal structures [19] and for the glassy-like carbon type G [13]

corresponding frequency limit is always lower (several orders of magnitude) than the conventional calculated frequency. So, at 2 Hz excitation frequency, our crystal can be considered as thermally very thick and consequently, the theoretical conditions are fulfilled.

The thermal parameters of all measured samples are given in Table 1. The thermal diffusivity values obtained from PPE and lock-in thermography are listed in separate rows. Each sample was measured three times and the resulted data were averaged. The thermal diffusivities measured with PPE technique are smaller than those measured by lock-in thermography for all specimens. Salazar et al. [7–9] have shown that the differences are mainly due to the presence of the coupling liquid between the sample and the sensor. Salazar et al. proposed a method in which transparent electrodes (ITO) are deposited on the sensor's surface ($LiTaO_3$), and a self-normalization procedure is used. In doing so, the thermal diffusivity of opaque solid samples can be measured with high accuracy. However, using the proposed method, each sample has to be measured in both back and front configurations.

The thermal effusivities listed in Table 1 represent the average value of effusivities computed at two excitation frequencies (3 and 5 Hz, respectively). The obtained values lie within 10 % deviation of the mean. The contour maps shown in Fig. 7 represent the precision of the fit performed with Eq. 8 to the experimental data obtained for ZnSe (a) and CdSe (b) crystals, respectively. The *x*-axis represents the error in the absolute value of the thickness of the coupling fluid. This absolute value is not known, only the thickness variation. The *y*-axis represents the thermal effusivity. The shape of the contour lines indicates the accuracy of the results. Contour lines extended along *Ox* axis indicate a good precision in thermal effusivity measurement. If they extend along *Oy* axis, the accuracy in the measurement of thermal effusivity is low. Circles mean similar accuracy in obtaining both thermal effusivity and location of the backing position. Our expertise indicates that the accuracy of this type of investigations increases if

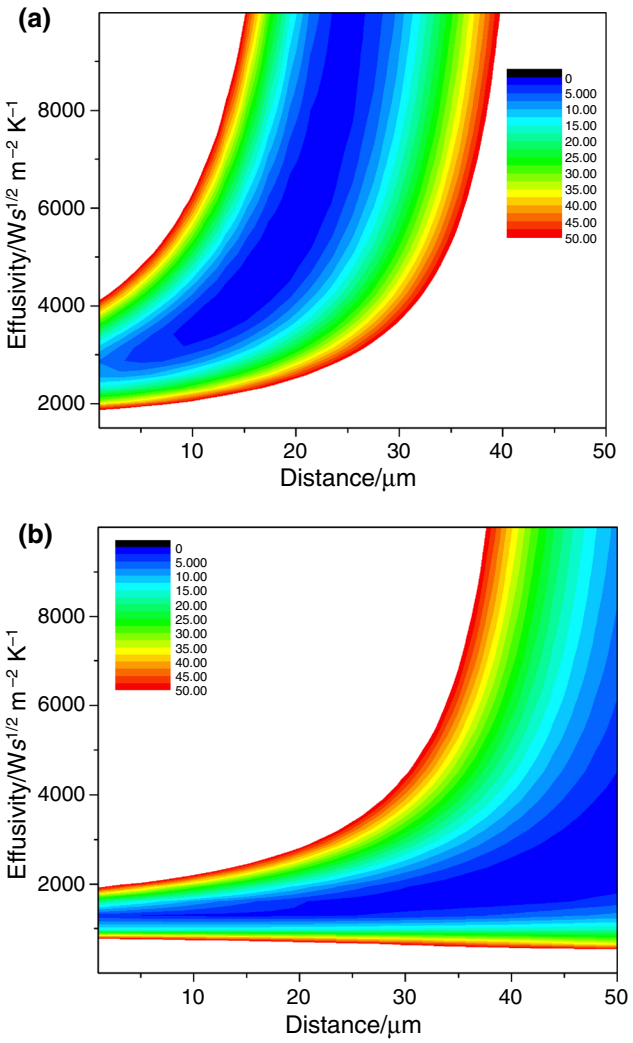


**Fig. 7** Contour maps of the precision of the fittings performed with Eq. 4 to the experimental data obtained for ZnSe (**a**) and CdSe (**b**) samples, respectively

the effusivity ratio coupling fluid/backing material goes to 1. One can see in Fig. 7 that for high backing/liquid ($e_3/e_2$) effusivity ratios, an accurate location of the backing

material is obtained, while thermal effusivity is obtained with low precision. This is the case of ZnSe sample, where $e_3/e_2$ (5,300/890 W $s^{1/2}$ $m^{-2}$ $K^{-1}$) is about 6. For CdSe sample, the ratio is two times smaller and consequently, the precision in thermal effusivity determination increases.

It is well known that the thermal diffusivity $\alpha$, effusivity $e$, density $\rho$, and mass specific heat $C$ are connected by two relationships: $\alpha = k/(\rho C)$ and $e = (k\rho C)^{1/2}$. Consequently, using these relationships, one can obtain the thermal conductivity $k$ and mass specific heat $C$. The density of the samples was estimated from their mass and volume. The thermal diffusivity used for calculation of other thermal parameters was taken as average value of the results obtained from PPE and infrared imaging techniques. The thermal conductivities of the II–VI binary crystals are rather different from the literature [19]. Nevertheless, the values obtained for glassy-like carbon are in good agreement with the literature data [13]. The thermal conductivity ($k = 6.34$ W $m^{-1}$ $K^{-1}$) of the reference sample (GC) is in very good agreement with the data from the producer ($k = 6.3$ W $m^{-1}$ $K^{-1}$). The specific heat of glassy-like carbon, found by Pawlak et al. [11] from differential scanning calorimetry (1,050 ± 2–5 % J $kg^{-1}$ $K^{-1}$) is in very good agreement with the result obtained in this work (1,075.1 J $kg^{-1}$ $K^{-1}$).

Thermal parameters strongly depend on the fabrication process, in contrast to optical properties. The energy gaps of the investigated crystals have been measured with photoacoustic spectroscopy (using piezoelectric detection) [20]. The obtained values of the optical parameters were consistent with the literature data. The quality of the crystal structure, the defects, and the concentration of impurities strongly influence the thermal properties of semiconductors. The reported reference values of the thermal conductivity are obtained for very pure crystal with low concentration of defects. Our samples were produced by Bridgman–Stockbarger method in which the obtained crystals are characterized by a high electrical resistance. It is known that the main source for this electrical resistance is the cation vacancies. One can reduce the concentration of these defects applying annealing procedure in cation vapor but our samples were grown without applying such a procedure. All these, together with the non-ideal measurement conditions (assumption of one-dimensional heat propagation, presence of the coupling fluid) can explain the observed discrepancies between the obtained values of thermal parameters and literature.

## Conclusions

In this paper, a complete thermal characterization of II–VI binary crystals (produced by high-pressure Bridgman method) was carried out. For this purpose, several different photothermal techniques have been applied. The thermal diffusivity of the samples was obtained by two investigation methods: BPPE technique and IR lock-in thermography. The thermal effusivities were measured using FPPE–TWRC method. The remaining two thermal parameters (thermal conductivity $k$ and specific heat $C$) have also been calculated. The thermal parameters obtained for the reference sample (GC) are in good agreement with the literature. Some inconsistencies between the thermal conductivity of the investigated crystals obtained in this study and the literature were found. In our opinion, this is mainly due to the fabrication process of the crystals and to the quality of their structure. Additional discrepancies can be generated by non-ideal measurements conditions, especially in BPPE configuration, where a thin (but uncontrolled) layer of coupling fluid is needed. To overcome this shortcoming, a non-contact technique as infrared lock-in thermography is suitable.

The PPE technique is able to find both thermal diffusivity and effusivity of the investigated semiconductors by combining the front and back configurations. In our opinion, the main advantage of the PPE method consists in its ability of directly measuring the thermal effusivity (in the front configuration) with high enough accuracy, using the TWRC scanning procedure that eliminates the influence of the coupling fluid. In the back configuration, the influence of the coupling fluid cannot be eliminated and, consequently, the values of the thermal diffusivity are underestimated. To tackle this problem, a non-contact technique, such as lock-in thermography, provides an interesting alternative investigation method. The main advantage of the lock-in thermography is that this technique allows a direct examination of the investigated surface, without using any coupling fluid. By applying the lock-in thermography detection, the unwanted DC component (extremely sensitive to the ambient temperature fluctuations and to the background reflections) is filtered out. The modulated components of the IR emission induced at the surface of the inspected sample by the thermal wave are then extracted with an excellent contrast (amplitude and phase images). Because the amplitude image is sensitive to the surface emissivity, whereas the phase image is independent on the quality of the surface and on the intensity fluctuation of the excitation source, the phase image always gives accurate results. For semi-transparent samples, the main drawback is a low absorption coefficient of the surface which will produce a very weak IR signal. To overcome this shortcoming, the surface must be blackened by a very thin conductive opaque layer (graphite). This additional conductive layer does not influence the results at the selected frequencies. In the same time, the requirements imposed by the particular detection case (punctual heat

source, thermally thick regime for the samples) must be fulfilled.

Considering the aim with which the present study was undertaken, it can be concluded that each method has its advantages and shortcomings, and thus a combination of a contact (PPE calorimetry) and non-contact (lock-in thermography) technique increases the accuracy in evaluating the thermal parameters of solids.

**Acknowledgements** The study was supported by the research fellowship within project "Enhancing Educational Potential of Nicolaus Copernicus University in the Disciplines of Mathematical and Natural Sciences" (project no. POKL.04.01.01-00-081/10.). Two authors (Mihaela Streza and Dorin Dadarlat) acknowledge partial financial support provided by the Ministry of Education Research and Youth of Romania, through the National Research Program PN-II-PT-PCCA-2-11-3.

## References

1. Niiyama Y, Watanabe M. BeMgZnSe-based ultraviolet lasers. Semiconduct Sci Technol. 2005;20:1187–97.
2. Rozpłoch F, Patyk J, Firszt F, Łęgowski S, Męczynska H, Zakrzewski J, Marasek A. Raman, photoluminescence and photoacoustic investigations of $Zn_{1-x-y}Be_xMn_ySe$ mixed crystals. Phys Stat Sol B. 2002;229:707–9.
3. Coufal H, Mandelis A. Pyroelectric sensors for the photothermal analysis of condensed phases. Ferroelectrics. 1991;118:379–409.
4. Dadarlat D, Chirtoc M, Candea R, Bratu I. Direct pyroelectric detection of optical absorption in non-transparent materials. Infrared Phys. 1984;24:469–71.
5. Dadarlat D. Contact and non-contact photothermal calorimetry for investigation of condensed matter. J Therm Anal Calorim. 2012;110:27–35.
6. Dadarlat D, Pop MN, Onija O, Streza M, Pop MM, Longuemart S, Depriester M, Sahraoui AH, Simon V. Photopyroelectric (PPE) calorimetry of composite materials. J Therm Anal Calorim. 2013;111:1129–32.
7. Salazar A. On the influence of the coupling fluid in photopyroelectric measurements. Rev Sci Instrum. 2003;74:825–7.
8. Salazar A, Oleaga A. A new method to overcome the underestimation of the thermal diffusivity of solid samples induced by the coupling fluid in photopyroelectric measurements. Int J Thermophys. 2012;33:1901–7.
9. Salazar A, Oleaga A. Overcoming the influence of the coupling fluid in photopyroelectric measurements of solid samples. Rev Sci Instrum. 2012;83:014903–7.
10. Shen J, Mandelis A. Thermal wave resonator cavity. Rev Sci Instrum. 1995;66:4999–5005.
11. Pawlak M, Firszt F, Łęgowski S, Męczyńska H, Gibkes J, Pelzl J. Thermal transport properties of Cd1 − xMgxSe mixed crystals measured by means of the photopyroelectric method. Int J Thermophys. 2010;31:187–98.
12. Dadarlat D. Photopyroelectric calorimetry of liquids; recent development and applications. Laser Phys. 2009;19:1330–9.
13. http://www.htw-gmbh.de/. Accessed 8 Jan 2014.
14. Chirtoc M, Mihailescu G. Theory of the photopyroelectric method for investigation of optical and thermal materials properties. Phys Rev B. 1989;40:9606–17.
15. Mandelis A, Zver MM. Theory of photopyroelectric spectroscopy of solids. J Appl Phys. 1985;57:4421–30.
16. Dadarlat D, Streza M, Pop MN, Tosa V, Delenclos S, Longuemart S, Sahraoui AH. Photopyroelectric calorimetry of FPPE–TWRC method. J Therm Anal Calorim. 2010;101:397–402.
17. Carslaw HW, Jaeger JC. Conduction of heat in solids. 2nd ed. London, UK: Oxford Univ. Press; 1959.
18. Chirtoc M, Antoniow J S, Egee M. The effective thermal thickness: a new concept for photothermal investigation of layered systems. AIP Conference Proceedings Rome, Italy. 1998; 463:84–86.
19. Madelung O. Semiconductors: data handbook. Berlin: Springer-Verlag; 2003.
20. Strzałkowski K, Zakrzewski J, Maliński M. Determination of the exciton binding energy using photothermal and photoluminescence spectroscopy. Int J Thermophys. 2013;34:691–700.